Well-Ordered $V_2O_5(001)$ Thin Films on Au(111): Growth and Thermal Stability

**Sébastien Guimond,[†] Jacobus M. Sturm, Daniel Göbke, Yuriy Romanyshyn,
Matthias Naschitzki, Helmut Kuhlenbeck,* and Hans-Joachim Freund**

*Fritz-Haber-Institut der Max-Planck-Gesellschaft, Department Chemical Physics, Faradayweg 4-6,
D-14195 Berlin, Germany*

Received: February 6, 2008; Revised Manuscript Received: May 5, 2008

Vanadium oxide thin films were grown on Au(111) by the oxidation of vapor-deposited V layers with 50 mbar of oxygen. The structure, composition, and thermal stability of the films have been investigated with scanning tunneling microscopy, low energy electron diffraction, photoemission spectroscopy, near-edge X-ray absorption fine structure, and temperature-programmed desorption. Well-ordered $V_2O_5(001)$ thin films containing very few point defects have been obtained. Although the films have the tendency to grow in large crystallites and "dewet" the interface layer, growth by multiple steps of V deposition and oxidation precludes this problem and leads to flat films having a surface with a low density of steps. The films are composed of rather large (~20 nm), single crystalline, and (001)-oriented V_2O_5 domains which show some azimuthal disorder between themselves. The X-ray-induced surface reduction of the $V_2O_5(001)$ films was investigated with STM. O vacancies do not form randomly on the surface but rather appear as pairs or rows, indicating a concerted reduction process. Upon heating in UHV, the films are stable up to 500 °C, and they start sublimating above this temperature. Significant thermally induced reduction of the films only occurs above 560 °C. Comparison between these results and published studies emphasizes the influence of surface contamination and beam damage on the thermal reduction of V_2O_5.

Introduction

Vanadium pentoxide (V_2O_5) thin films are of considerable scientific and technological interest. For instance, they have potential uses in electrochromic devices[1,2] and lithium microbatteries.[3,4] These applications rely on the good intercalation properties of the orthorhombic V_2O_5 crystal structure. V_2O_5 finds its most important application in the chemical industry, where it is used as an oxidation catalyst. Examples of catalytic processes involving V_2O_5-based catalysis include the oxidation of SO_2 to SO_3 and the selective oxidation of various hydrocarbons.[5–8] The catalysts usually consist of V_2O_5 supported on another oxide such as SiO_2, Al_2O_3, TiO_2, or ZrO_2. They are often referred to as "monolayer catalysts" assuming that the V_2O_5 forms a monolayer film on the support material.[6,9] In spite of their importance, many questions about the atomic structure and the reaction mechanisms at the surfaces of these highly complex systems remain unanswered. Developing a better understanding of supported vanadium oxide catalysts is not only of general scientific interest but is also useful for the development of new applications and materials. A useful approach to gain insight into these problems is the use of well-defined model surfaces, systems that are much simpler and that can be studied at the molecular level using the range of surface science techniques that are nowadays available. The (001) surface of V_2O_5 single crystals is a relevant model system, and it has been the subject of experimental and theoretical studies.[5,10] Although such single crystals can be grown, their preparation is involved and time-consuming.[11] They are also sensitive to beam damage[12–14] and must therefore be cleaved frequently when electron-based surface science techniques are applied, which is uncomfortable and can be a problem in view of the small crystal sizes. To avoid these complications, the possibility of growing well-ordered V_2O_5 thin films would be advantageous. This was the motivation for the present study.

Various methods have been used to grow V_2O_5 thin films, including flash-evaporation of V_2O_5,[15,16] pulsed-laser deposition,[17] magnetron sputtering,[18,19] chemical vapor deposition,[20] and spray pyrolysis.[21] However, in many of these cases substoichiometric films (i.e., containing some V^{4+} species) were obtained. Several films were also amorphous or polycrystalline at best. More generally, the growth of well-ordered, flat V_2O_5 films suitable for reactivity model studies has not been reported yet. In the present work, we have used the oxidation of physical vapor deposited (PVD) V layers with O_2 as a relatively simple and cheap method to grow V_2O_5 films in a well controlled manner. Vanadium pentoxide is the oxide with the highest vanadium oxidation state in the vanadium−oxygen system, and the oxidation of V to V_2O_5 requires O_2 pressures that are not suitable for ultra high vacuum (UHV) systems. This has been evidenced by several studies, where it was shown that the preparation of films by reactive evaporation or postdeposition oxidation of V under oxygen pressures in the $10^{-7}-10^{-6}$ mbar range results in the formation of oxides having a V^{3+} or V^{4+} oxidation state (see refs 22–27 for instance). Wong et al. investigated the formation of ultrathin (approximately monolayer) oxide films by oxidation of vapor-deposited V in 10^{-3} mbar O_2.[28] They reported that the resulting films contained primarily V^{5+} ions but also a fraction of V^{4+} species. To circumvent this limitation, we have used a dedicated high pressure cell to carry "*in situ*" (i.e., without exposure to ambient atmosphere) the oxidation of V in 50 mbar O_2.

We recently reported on the growth of ultrathin V_2O_y ($y \sim 5$) films using the same preparation method.[29] Results showed

---

* Corresponding author. Phone: +49 30 8413 4222. Fax: +49 30 8413 3155. E-mail: kuhlenbeck@fhi-berlin.mpg.de.

[†] Current address: Empa. Swiss Federal Laboratories for Materials Testing and Research, Lerchenfeldstr. 5, CH-9014 St. Gallen, Switzerland.

10.1021/jp8011156 CCC: $40.75

that well-ordered coincidence monolayer structures with a $V^{\sim 5+}$ oxidation state can be obtained after oxidation of submonolayer amounts of vanadium. Upon oxidation of slightly higher quantities of V, a two layer-thick film having a surface structure similar to $V_6O_{13}(001)$ was obtained. It was finally shown that the formation of this $V_6O_{13}(001)$-like film precedes the growth of $V_2O_5(001)$ crystallites at higher thicknesses. In the present paper, we report results concerning the growth of thicker layers. The structure and the composition of the films have been studied with scanning tunneling microscopy (STM), low energy electron diffraction (LEED), photoemission spectroscopy (PES), and near-edge X-ray absorption fine structure (NEXAFS). It is shown that flat and well-ordered $V_2O_5(001)$ thin films can be grown. Although the films have some azimuthal disorder, they consist of large (001)-oriented crystalline domains that have very few point defects. In the course of the experiments, the surface reduction of the $V_2O_5(001)$ films during XPS analysis was verified with STM. The results suggest that exposure to X-rays creates vanadyl ($V{=}O$) oxygen atom vacancies. These vacancies appear to be somewhat grouped together, forming rows along [010] and pairs along [100]. This observation partly confirms the results of the calculations made by Ganduglia-Pirovano and Sauer.[30]

In the context of model reactivity studies, the thermal stability of the V_2O_5 surfaces under UHV conditions is an important factor that has to be taken into account. For that reason, we also investigated the $V_2O_5(001)$/Au(111) thin films with thermal-programmed desorption (TPD). The films are found to start sublimating at a temperature of about 500 °C, whereas significant loss of oxygen only occurs at ~560 °C or above. The results reported in the literature concerning the reduction of V_2O_5 under UHV are briefly reviewed and compared to our findings. The considerable discrepancies existing between some of the various published studies are interpreted on the basis of the influence of contamination and beam damage on the reduction of V_2O_5.

Experimental Methods

The UHV systems in which the experiments have been carried-out and the preparation of the thin films have been described in details elsewhere.[29] The main characteristics are briefly summarized here. Most of the experiments were performed in a commercial UHV system with a base pressure $<1 \times 10^{-10}$ mbar (Omicron). This system contains facilities for sample preparation (sputtering, vanadium evaporation) and surface characterization with XPS, LEED, TPD, and STM. The NEXAFS and valence band photoemission spectroscopy experiments were carried out in another UHV system connected to the UE52-PGM undulator beamline of the BESSY II synchrotron radiation center in Berlin. This system is equipped with a Scienta SES200 hemispherical electron analyzer for PES and standard sample cleaning/preparation equipment. In both UHV systems, the sample holder can be transferred without exposure to air between the analysis/preparation chamber and the high pressure cell, the latter being connected directly to the chamber via a gate valve. The sample holder, which consists of a small plate, holding clamps, and some thermocouple connectors, is mostly built using platinum parts to avoid extensive oxidation/oxygen adsorption or any gas phase transport of oxide from the holder to the sample surface during the high pressure (50 mbar) oxidation.

The Au(111) sample was cleaned by cycles of Ar^+ sputtering (4000 eV, ~7 μA) at room temperature and annealing at 700 °C for 20 min in UHV. This procedure was repeated several time until no contaminants were detected using XPS and extended terraces displaying the Au(111) herringbone reconstruction[31] could be observed with STM. For a clean and well-ordered surface, diffraction spots pertaining to the reconstruction could also be observed in the LEED pattern.

The films were grown by first evaporating a given quantity of metallic vanadium onto Au(111) in UHV and then transferring the sample into the high pressure cell to carry out the oxidation procedure. Vanadium was evaporated with an Omicron EFM3 electron beam evaporator while the Au(111) substrate was kept at room temperature. The evaporation rate was calibrated in situ with a quartz crystal microbalance (in both UHV systems) and with STM images taken after evaporation. The evaporation rate was typically ~0.4 Å/min (0.2 MLE/min). The deposited V thicknesses are reported here in monolayer equivalent (MLE), where 1 MLE contains the same number of V atoms as one layer of Au(111) ($\sim 1.39 \times 10^{15}$ atoms/cm^2). The evaporated V layers were oxidized by heating the sample at 400 °C for 10 min under an oxygen flow (50 mbar) in the high pressure cell. The sample temperature was allowed to cool to about 100 °C before pumping down the high pressure cell and transferring the sample back to the main chamber. After oxidation of the films, no traces of surface contamination could be detected with XPS.

The XPS data were acquired using Mg Kα radiation (1253.6 eV) from a nonmonochromated source. An electron takeoff angle (θ) of 70° with respect to the surface normal has been used. The binding energy scale of the spectra was referenced to the Au4f$_{7/2}$ peak of the clean Au(111) substrate at 84 eV.[32] The spectra reported here are shown without subtraction of the background intensity, but they have been corrected for X-ray satellites using the routine supplied with the CasaXPS program.[33] STM images were recorded at room temperature in the constant tunneling current mode. Commercial etched Pt/Ir tips (Molecular Imaging) have been used. The STM scanner has been calibrated by imaging the unit cell of Au(111). In order to minimize the influence of X-ray or e-beam-induced reduction processes, the films were always first probed with STM. NEXAFS spectra were recorded by sweeping the energy of the linearly polarized light between 510 and 540 eV while measuring the current flowing between the sample and ground potential (total electron yield). Two different light incidence polar angles were used, 0° and 70°. Valence band photoemission spectroscopy was performed with a photon energy of 121 eV and a takeoff angle of 70°. TPD curves were recorded in the temperature range between room temperature (25 °C) and 680 °C with a VG Smart-IQ+ quadrupole mass spectrometer equipped with a pumped Feulner cup[34] to blind out most molecules not desorbing from the front side of the sample. Different m/z signals corresponding to O_2 (30) and various V_xO_y fragments (67: VO, 83: VO_2, 166: V_2O_4) have been monitored as a function of the sample temperature. Additionally, the evolution of the main chamber's pressure was recorded during the TPD runs. The sample was heated from the backside by electron bombardment, and its surface was positioned at a distance of about 1 mm in front of the nozzle entrance of the Feulner cup. A constant heating ramp of 0.5 °C/s has been used.

Some experiments were also performed with oxide films intentionally reduced by electron bombardment from a hot filament employing an electron acceleration voltage of 50 V. This rather small voltage was used in order to preferentially reduce the surface region and to not produce too many defects in region below the surface.

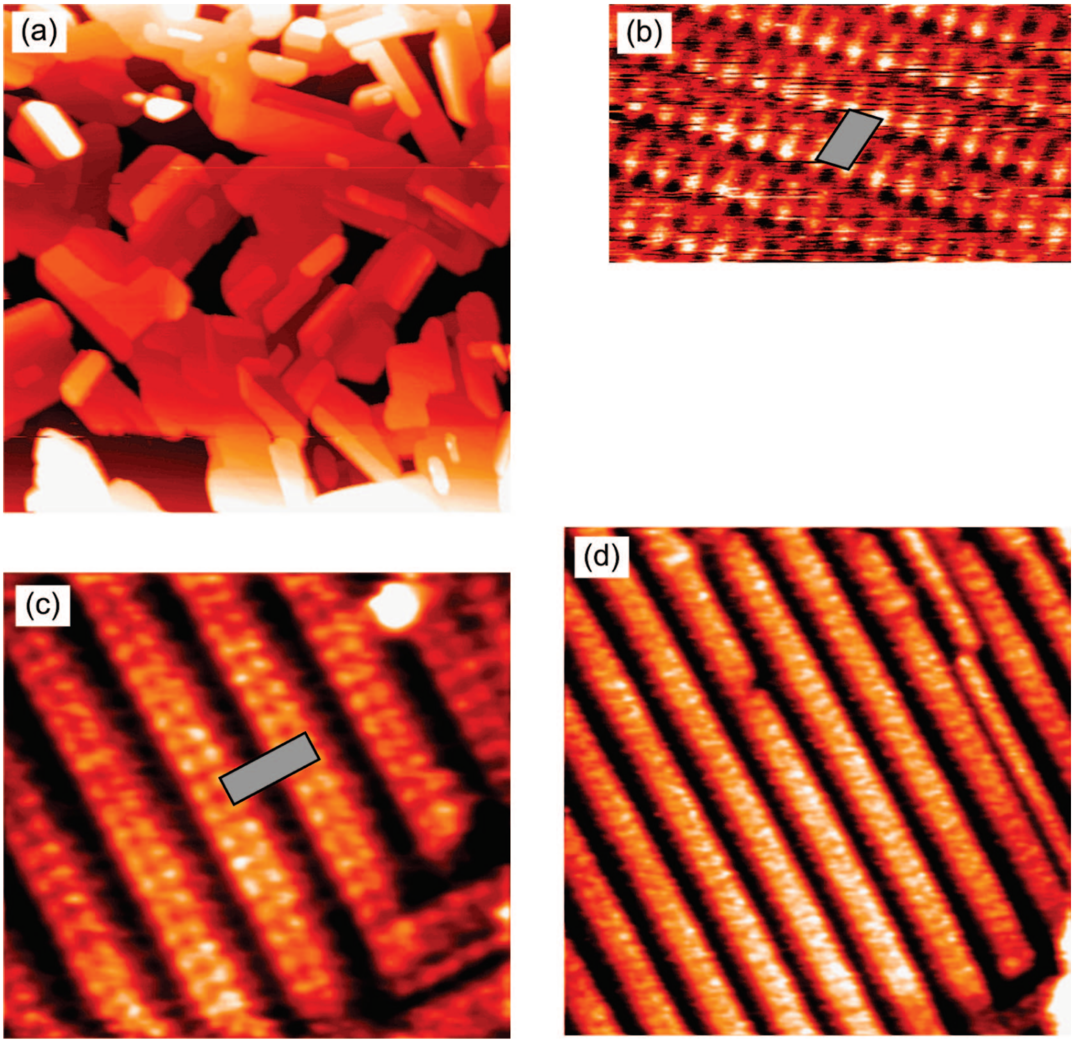

Figure 1. STM images of a film formed by the oxidation of 5.2 MLE V/Au(111) ((a): 300 nm × 300 nm, 3.5 V, 0.2 nA, (b): 5 nm × 2.8 nm, 3 V, 0.2 nA, (c): 6.3 nm × 5.8 nm, 2 V, 0.2 nA, (d): 10 nm × 10 nm, 2 V, 0.2 nA). Image b was acquired in one of the dark areas of image a, while images c and d are representative of the high features. In images b and c the surface unit cells are indicated by gray parallelograms.

Results and Discussion

a. Thin Film Growth and Characterization. As reported in ref 29 we have shown that small isolated $V_2O_5(001)$ crystallites start to grow after the completion of a two layers thick $V_6O_{13}(001)$-like interface (this was observed following the oxidation of about 1.56 MLE V/Au(111)). Thicker films have been investigated, and the results are discussed here. Figure 1a displays a large scale STM picture of a film obtained by the oxidation of 5.2 MLE V/Au(111). The quantity of vanadium that is required to complete a $V_2O_5(001)$ single layer is equal to about 0.7 MLE, which means that the oxidation of 5.2 MLE V would result in a V_2O_5 film thickness of ~7.4 mL (3.2 nm), assuming the growth of a uniform and ordered $V_2O_5(001)$ film and assuming that sublimation does not occur during oxidation. From the image, one can see that the V_2O_5 islands have coalesced to some extent and that rather big crystallites have formed. Also, the STM image reveals large darker areas that are about 4 nm deep, where the surface structure of the $V_6O_{13}(001)$-like interface could be resolved (Figure 1b). As indicated in Figure 1b, this structure is characterized by an oblique unit cell (3.6 Å × 6 Å, $\alpha = 73°$). This observation means that the V_2O_5 film does not fully cover the interface layer. However, the surface of the crystallites displays a well-ordered $V_2O_5(001)$ structure containing a low number of point defects. The crystalline structure of V_2O_5 projected along [010] is depicted in Figure 2a. V_2O_5 has an orthorhombic structure consisting of layers parallel to (001).[10,35,36] The V coordination is best described as distorted square pyramidal, and the layers are composed of VO_5 units that are sharing edges or corners in the (001) plane. For each square pyramid, the apical oxygen atom forms a double bond with the V atom, and these vanadyl groups ($V{=}O$) are oriented along [001] in alternating directions toward one of the next neighboring layers. The layers are considered to be held together by van der Waals $V{=}O\cdots V$ interactions. The arrangement of $V_2O_5(001)$ is shown in Figure 2b, where double rows of vanadyl O atoms are seen to extend along the [010] direction. This surface has a 3.56 Å × 11.52 Å rectangular unit cell. The double row structure and the unit cell characterizing $V_2O_5(001)$ are clearly visible in the high resolution STM images shown in Figures 1c,d. Some line defects are also occasionally observed, as seen in the upper-right corner of Figure 1d. The origin of the contrast in the STM images of $V_2O_5(001)$ has been debated in the past.[37–40] As can be seen in Figure 2b, the surface exposes both double rows of vanadyl groups and vanadium atoms (the two alternate along [100]). Authors have expressed various opinions concerning which one of the two features is really imaged in STM (especially as a function of the bias). STM observations of transition metal oxides are often interpreted by assuming that the empty-state images are dominated by the more electropositive atoms (metal)

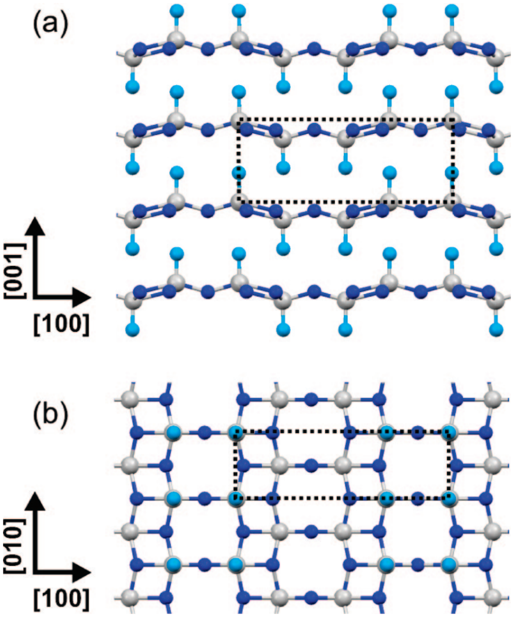

Figure 2. V_2O_5 crystal structure: (a) projected along [010] and (b) (001) surface. Unit cells are indicated by dotted lines. Blue and gray spheres correspond to O and V atoms, respectively. The vanadyl O atoms are represented by light blue spheres.

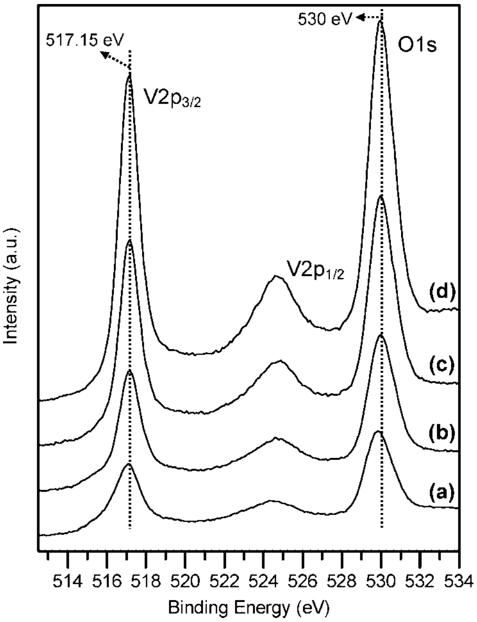

Figure 3. XP spectra (V2p and O1s region) of V_xO_y/Au(111) as a function of the V coverage initially deposited. (a): 1.04 MLE, (b): 2.08 MLE, (c): 5.2 MLE, (d): three successive depositions of 2.6 MLE V and oxidation cycles. In all cases, the intensity was normalized to the background signal at 500 eV (the spectra were afterward shifted with respect to each other along the *y* axis for display).

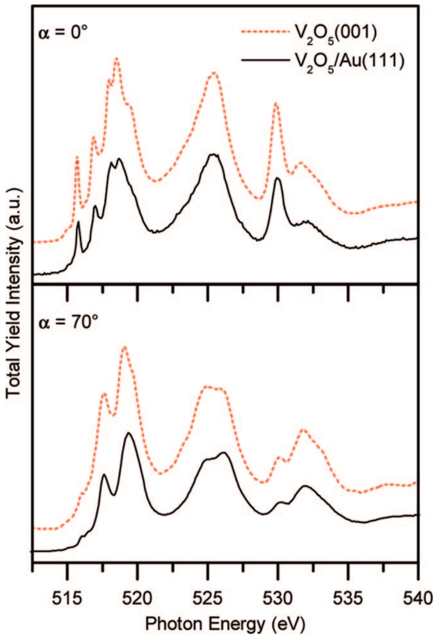

Figure 4. Comparison between the NEXAFS spectra obtained for a V_2O_5(001) single crystal and for a film formed by the oxidation of about 2.6 MLE V/Au(111). The spectra were acquired at two different light incidence angles (α), 0° and 70°.

and that the filled-state images are rather influenced by the electronegative atoms (oxygen). In the case of V_2O_5, the valence and the conduction bands are indeed dominated by O2p and V3d states, respectively. On the basis of this, different groups assigned the features observed in the positive bias (empty-states) STM images to the double rows of exposed vanadium atoms.[37,38] Intuitively this might seem reasonable, but there are good arguments supporting the opposite. First, one has to consider that in V_2O_5 the conduction and valence bands are formed by *hybridized* O2p and V3d orbitals.[41,42] Also, for the rather high biases used here the electrons tunnel in the upper part of the conduction band where the contribution of O2p states is relatively high.[39] The main reason why the exposed $V{=}O$ groups could be responsible for the STM contrast is actually a geometric argument: the vanadyl oxygen atoms stick out of the surface; the oxygen atoms of the vanadyl groups are about 2 Å higher than the vanadium atoms of the vanadium rows. Because of V3d+O2p hybridization there will be unoccupied density of states near to the position of the vanadyl oxygen cores and tunneling may occur into these states. Since these states stick out of the surface, they may appear more prominent in the STM images than states related to the vanadium rows between the vanadyl double rows. In agreement with calculations performed by Smith et al.[39,40] and with observations made for V_2O_3(0001) on Au(111)[43] we assign the bright protrusions in the STM images shown in Figure 1c and 1d to the vanadyl groups on the V_2O_5(001) surface. Accordingly, occasional missing bright protrusions (see the middle-top part of Figure 1d) are attributed to vanadyl O vacancy point defects. The XP spectrum corresponding to this film (oxidation of 5.2 MLE V) is displayed in Figure 3 (spectrum c). As expected for V_2O_5, the V2p3/2 peak appears at a binding energy of 517.15 eV.[44–47] A small shoulder also seems to be present on the low binding energy side of the peak, suggesting the presence of some V atoms with a lower oxidation state in the film. This extra intensity might in part come from the surface areas where the interface layer is exposed (see spectrum a, which corresponds to the V_6O_{13}(001)-like interface film[29]). Indeed, for thinner V_2O_5(001) layers a greater fraction of the interface is uncovered and the shoulder at lower binding energy is more prominent (see spectrum b in Figure 3). However, as discussed below, some surface reduction during the XPS analysis cannot be excluded and probably also contributes to the intensity of the shoulder.

The V_2O_5 films were also characterized with angle-resolved NEXAFS. The results are shown in Figure 4 for a film produced by the oxidation of 2.6 MLE V/Au(111) together with V_2O_5(001) single crystal data on the same graphs. The spectra are almost identical, confirming the attribution of the film structure to V_2O_5. NEXAFS is sensitive to the orientation of

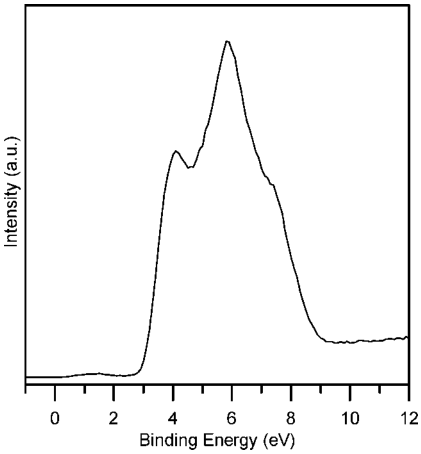

Figure 5. Valence band photoemission spectrum of a film formed by the oxidation of 2.6 MLE V/Au(111).

the interatomic bonds in materials since the transition matrix elements determining the X-ray absorption intensity are related to the relative orientation between the molecular bonds and the E-vector of the exciting beam. The fact that the intensity of the various bands has the same variation as a function of the light incidence polar angle then also proves that the film is indeed (001)-oriented. Small differences between the two sets of spectra can originate from contributions of the interface layer. Also, although the single crystal data were recorded for a defined azimuthal orientation, those corresponding to the thin films are intrinsically acquired over an average of different azimuthal angles (this is due to some rotational disorder in the thin film, see below). This has probably an effect since some small variations in the NEXAFS spectra of $V_2O_5(001)$ single crystals are expected as a function of the azimuthal orientation.[48]

The fact that the thin films grow with their [001] crystallographic axis oriented parallel to the surface normal is not very surprising. Indeed, the weakly interacting layers constituting V_2O_5 are stacked along this direction, and it is rather straightforward to see that the (001) plane is the surface with the lowest free energy of this crystal structure (a calculated value of 0.040 J/m^2 has been reported[30]). This explains why V_2O_5 has a higher tendency to expose its (001) surface, an effect which is experimentally commonly observed for single crystals[11] and powder particles.[49] As a matter of fact, it seems that V_2O_5 films have a tendency to grow with a preferred (001) orientation regardless of the nature of the substrate (this was for instance reported for amorphous glass[21]). Considering this, it would be tempting to describe the growth of $V_2O_5(001)$ thin films in terms of van der Waals epitaxy.[50] This growth mode was observed for other compounds made of layers interacting by van der Waals forces like transition metal dichalcogenides (MoS_2, $NbSe_2$, etc). In this case, ultrathin films can grow with their own lattice constant on various (unreactive) substrates, even under the existence of very large lattice mismatch. The present case is however slightly different, as an interface layer with a dissimilar structure first grows on Au(111) before the regular $V_2O_5(001)$ sheets start to form. This is in contrast to the MoS_2/Au(111) system, where a regular $MoS_2(0001)$ structure was observed for monolayer-thick nanocrystallites.[51]

It has been mentioned before that very few oxygen vacancy point defects could be observed with STM. This conclusion was further evidenced with valence band photoemission spectroscopy. A spectrum is shown in Figure 5 for a film formed after the oxidation of 2.6 MLE V/Au(111). The broad features between ~3 and 9 eV are due to emission from oxygen and vanadium levels in the oxide band structure, and their general shape corresponds rather well to the one observed for UHV-cleaved $V_2O_5(001)$ single crystals.[52,53] The low abundance of not fully oxidized vanadium atoms can be judged from the nearly vanishing emission intensity in the binding energy range between the Fermi edge and 3 eV. The emission from the V3d levels of not fully oxidized vanadium atoms would show up in this spectral region.[44] Obviously, in the present case only a very faint signal can be observed. It can even be argued that some of this intensity comes from radiation-induced reduction occurring during the acquisition of the spectrum.

The growth of "closed" $V_2O_5(001)$ films that do not expose interface areas is important for adsorption/reactivity studies. For such investigations it could otherwise be difficult to disentangle the spectroscopic signal coming from molecules adsorbed on the various surfaces: interface layer, surface, and side facets of the $V_2O_5(001)$ crystallites. For films prepared by the oxidation of V layers with thicknesses ranging from 1.56 to 5.2 MLE, some interface area was always left uncovered. It also appeared that between 3.15 and 5.2 MLE V, this area stayed more or less constant and that mainly the height of the $V_2O_5(001)$ crystallites increased. This effect could be due to Ostwald ripening occurring during the oxidation process which would result in the growth of bigger crystals at the expense of the smaller ones. It was possible to avoid this problem by growing the films in multiple V evaporation/oxidation steps. Figure 6a shows a large scale STM image corresponding to a film prepared by the sequential evaporation and oxidation of three 2.6 MLE V layers. The conditions used for the oxidation were the same as the ones used for the other films (400 °C, 50 mbar O_2, 10 min). Several of these large scale images could be recorded at various places on the sample surface, and in all the cases no exposed interface was observed. The majority of steps seen in Figure 6a has a height corresponding to one $V_2O_5(001)$ layer (~4.4 Å). As evidenced in Figure 6b, the surface also displays rather large single crystalline domains and very few point defects. However, the size of the domains is perhaps a bit smaller than in the case of the films grown in one evaporation/oxidation step, and a number of grain boundaries plus some occasional screw dislocations can be observed. Considering that ~0.7 MLE V is required to complete a $V_2O_5(001)$ single layer, this film is expected to have a thickness of about 11 layers, i.e. 4.8 nm (since the unit cell vector along [001] has a length of 4.37 Å,[36] see Figure 2a).

A possible reason why the morphology is different if the layer is grown in several steps would be that evaporated *metallic* V layers grow differently on top of an existing V oxide film and on gold. It may be assumed that metallic V on vanadium oxide is flatter and more dispersed than on Au due to a stronger interaction with the oxide surface (the evaporated metal atoms can interact with the oxygen atoms of the oxide and form chemical bonds). This would then provide a different starting point for the growth of crystallites via atomic rearrangement within crystallites, coalescence of crystallites, and Ostwald ripening during the oxidation procedure at elevated temperature and could delay the formation of very big islands and uncovered interface areas. The fact that the films grown in multiple steps were always flatter was also confirmed by the higher damping of the substrate's core levels signal observed in the XPS data.

The LEED patterns of the $V_2O_5(001)$/Au(111) thin films show rings instead of spots (this is shown in Figure 6c for a film formed by the deposition/oxidation of three 2.6 MLE V layers). Such an observation means that the [001]-oriented crystalline

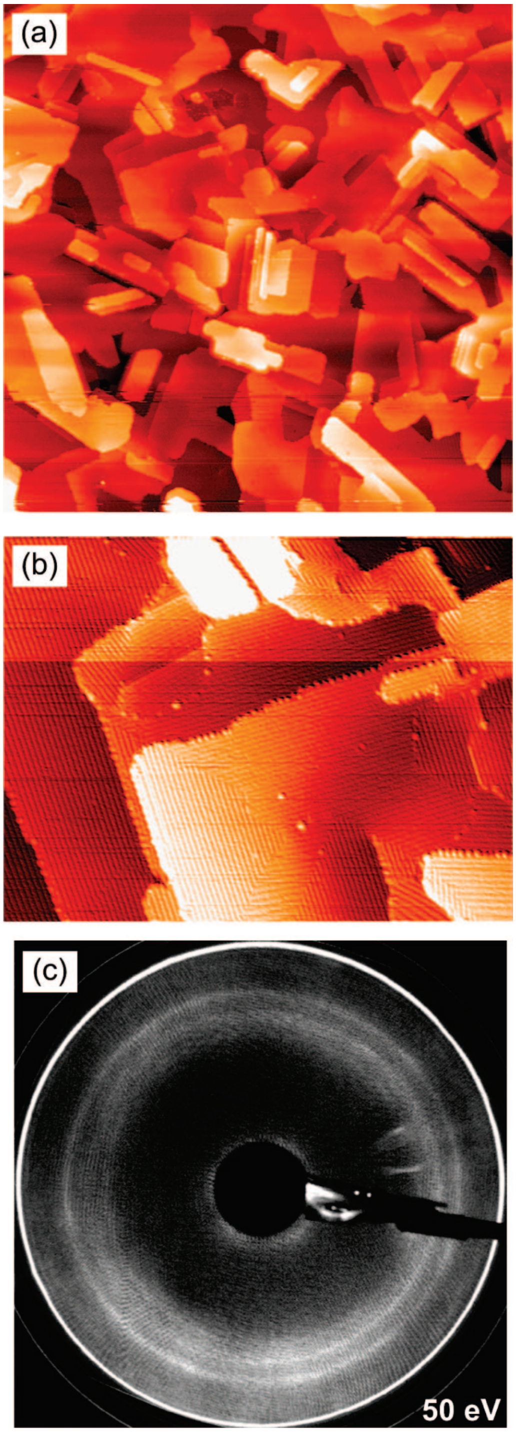

Figure 6. STM images ((a): 300 nm × 300 nm, 3.5 V, 0.2 nA, (b): 100 nm × 75.8 nm, 3 V, 0.2 nA (differentiated)), and LEED pattern (c) obtained for a film formed by three successive depositions of 2.6 MLE V and oxidation cycles.

domains composing the film have random azimuthal orientations. This can also be observed in the STM image shown in Figure 6b. Rotational disorder was also observed for the interface layer, and it has been attributed to a rather weak interaction between the growing film and the substrate.[29] Since STM reveals well ordered surfaces, the background intensity in the diffraction pattern seen in Figure 6c is mostly ascribed to electron beam-induced reduction of the film during the LEED experiment. In fact, it is well-known that V_2O_5 is sensitive to electron beams.[12,13] In the present case, this reduction was obvious as the LEED pattern would fade away in only a few seconds. The same observation was reported for V_2O_5 single crystals.[53]

The closed films were also characterized with XPS. A spectrum corresponding to a film grown in three evaporation/oxidation steps (3 × 2.6 MLE V layers) is shown in Figure 3 (spectrum d). The spectrum displays rather sharp V2p3/2 and O1s peaks positioned at binding energies of 517.15 and 530 eV, respectively, and is very similar to spectra reported previously for V_2O_5 (see ref 47 for instance). Nevertheless, the V2p peaks cannot be fitted with only one component, and an extra weak peak has to be accounted for on their lower binding energy side. In other words, a small fraction of reduced V species is present on the surface. This can likely be attributed for the most part to X-ray-induced reduction taking place during the analysis. The reduction of V_2O_5 by X-ray exposure was investigated by Chenakin et al., who concluded that XPS recorded with parameters similar to the ones that we employed induces the rapid formation of a small fraction of V^{4+} species on the surface.[14] X-ray-induced damage in oxides is believed to be mainly caused by electron−hole pair creation and Auger decay.[54] The multiple hole states created in the valence band by Auger decay can break bonds between V and O, leading to the reduction of vanadium atoms and to the desorption of oxygen. This damage is hard to avoid, and the observation of small amounts of reduced V species at the surface of V_2O_5 with XPS is thus rather common.[13,47,53] STM images taken after the XPS analysis of the film (Figure 7) clearly reveal this effect. During the analysis, the sample was exposed to Mg Kα radiation for about 90 min, the X-ray source being operated at a power of 260 W. Compared to the pictures obtained for the same film before X-ray exposure (Figure 6), dark features are now distributed on the vanadyl oxygen double rows. The presence of significant amounts of C-containing adsorbates, OH, or H_2O on this surface can be excluded based on the XPS results: no intensity could be detected in the C1s region (not shown here). Also, hydroxyl groups or adsorbed water molecules would give rise to O1s intensity in the binding energy range between 531 and 533 eV,[55] which was not observed here (see Figure 3, spectrum d). Single missing bright protrusions (dark spots) in the STM images of as-prepared $V_2O_5(001)$ thin films have already been attributed to missing vanadyl O atom point defects (for reasons mentioned above). Similarly, the darker areas of the double rows in Figure 7 can be assigned to groups of missing vanadyl O atoms. The images clearly reveal that the vacancies are not distributed randomly on the surface, and they mostly appear somewhat grouped together. Similar observations have been made by Smith et al. for cleaved single crystals (which, in their experiments, apparently showed some degree of reduction).[39] In Figure 7c, the positions of the missing oxygen atoms seen in Figure 7b are highlighted by gray asterisks (whereas the surrounding remaining vanadyl O are indicated by blue circles). Vacancies are seen to form pairs along [100] and/or rows along [010]. The formation of oxygen vacancies at the surface of $V_2O_5(001)$ has been investigated with density functional theory by Ganduglia-Pirovano and Sauer[30] and by Hermann et al.[56] Their results show that the vacancy formation energy is much lower for vanadyl oxygen than for 2- and 3-fold coordinated surface oxygen atoms. The calculations of Ganduglia-Pirovano and Sauer also predicted that the reduced V cations (resulting from the loss of the vanadyl O atom) are stabilized by relaxation, where the cation moves downward and forms a bond with a vanadyl oxygen of the layer underneath. This relaxation lowers the vacancy formation energy for the neigh-

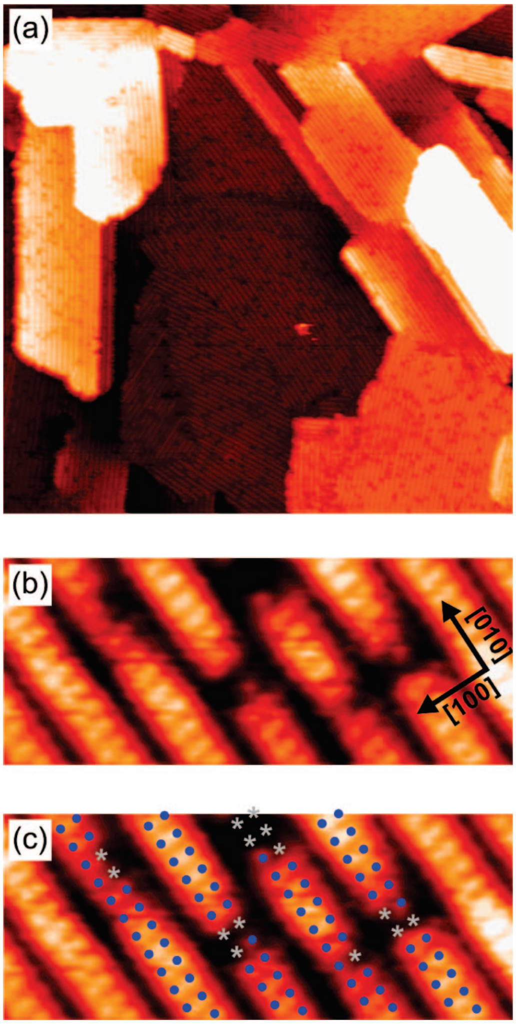

Figure 7. STM images ((a): 100 nm × 100 nm, 3 V, 0.2 nA, (b and c): 7.7 nm × 3.1 nm, 3 V, 0.2 nA) of a $V_2O_5(001)$ film exposed to Mg Kα X-rays (film formed by three depositions/oxidation cycles of 2.6 MLE V). Image c is a copy of image b, where the missing and remaining vanadyl O atoms are respectively indicated with asterisks and circles.

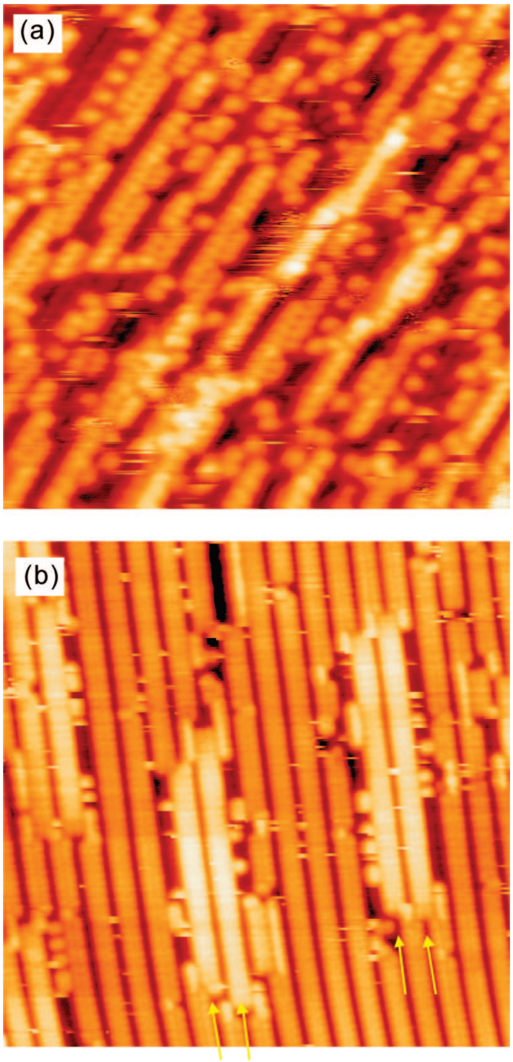

Figure 8. (a) STM image of a V_2O_5 film after electron bombardment (dose 10 mC), 10 nm × 10 nm, 1.5 V, 0.2 nA, (b) after annealing to 287 °C for 2 min, 20 nm × 20 nm, 2.5 V, 0.2 nA, the arrows indicate stacking faults.

boring surface *V*═O oxygen atoms, resulting in a concerted reduction of the surface. Their results indeed predict that upon reduction of the surface, missing rows along [010] will preferentially form. On the other hand, the calculations suggest that vacancy pairs along [100] (one vacancy on each side of a double row) would have a *higher* formation energy than single vacancies. Interestingly, for the experimental parameters used here such missing vanadyl O vacancy pairs appear to be very common.

Triggered by the results discussed above, V_2O_5 films were intentionally reduced by electron bombardment, and the thermal behavior of the reduced layers was investigated. Figure 8a and 8b show STM images obtained after bombarding a film (from 3 × 3.1 MLE vanadium) with an electron dose of 10 mC (a) and after annealing the reduced film for 2 min at 287 °C (b). Whereas the nonannealed reduced surface cannot be recognized as V_2O_5 anymore, large parts of the surface are recovered after annealing. This can be attributed to diffusion of oxygen from deeper layers toward the surface.[57] For lower reduction doses, this surface healing is almost perfect (not shown here), whereas in the current case stacking faults arise as indicated by arrows. From Figure 8b one might get the impression that these stacking faults consist of vanadyl groups pointing upward at positions where they would point downward on the nonfaulted surface. Of course, without STM intensity calculations or additional experimental evidence this remains speculation.

By repeated cycles of surface reduction and annealing the subsurface layers can be depleted of oxygen. Figure 9 displays STM images of a film subjected to four cycles of reduction (total electron dose: 60 mC) and annealing at 217 °C for 2 min, followed by a final anneal at 577 °C for 2 min to order the film. As will be shown later, at this temperature the oxide layer does not just lose oxygen but also some vanadium. Figure 9b shows a part of the bottom area in Figure 9a. To enhance the visibility of the details, this image was Fourier filtered and it shows a V_6O_{13}-type structure similar to the one shown in Figure 1b. The upper part of Figure 9a exhibits V_2O_5-type structures as is obvious from the vanadyl double rows. A possible explanation for the V_6O_{13}-type structure in the lower part of Figure 9a could be that the interface layer gets exposed due to dewetting and partial sublimation of the V_2O_5 film. However, the steps in the V_6O_{13} area are about 6 Å high, which is significantly larger than the step size on Au(111), demonstrating that the V_6O_{13}-type area in Figure 9a is not to be attributed to the interface layer but to the reduction of the $V_2O_5(001)$ layer. After an additional cycle of reduction with an electron dose of

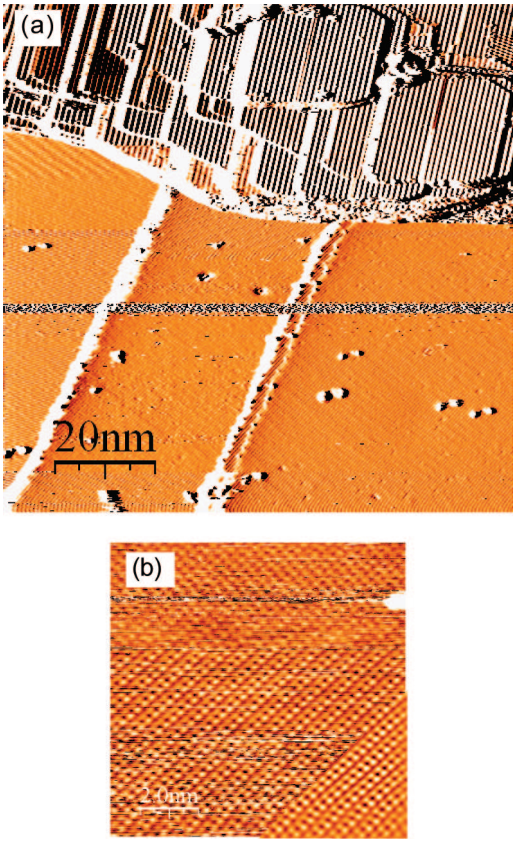

Figure 9. (a) Differentiated STM image (100 nm × 100 nm, 2.5 V, 0.2 nA) of a V_2O_5 film, exposed to a total electron dose of 60 mC, followed by annealing up to 577 °C for 2 min. (b) High resolution scan (10 nm × 10 nm, 2.5 V, 0.2 nA) of a V_6O_{13} area, the bottom-right corner has been FFT filtered for clarity.

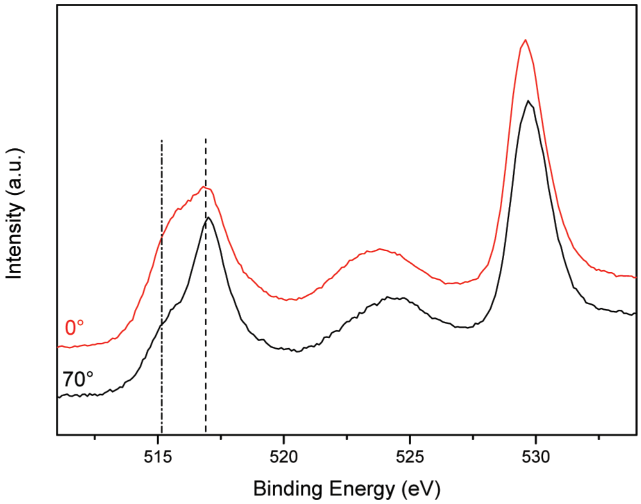

Figure 10. XPS spectra of a V_2O_5 film exposed to reduction/anneal cycles for two angles between the surface normal and analyzer axis. The dashed line indicates the binding energy of V_6O_{13} and the dashed-dotted line that of V_2O_3.[45]

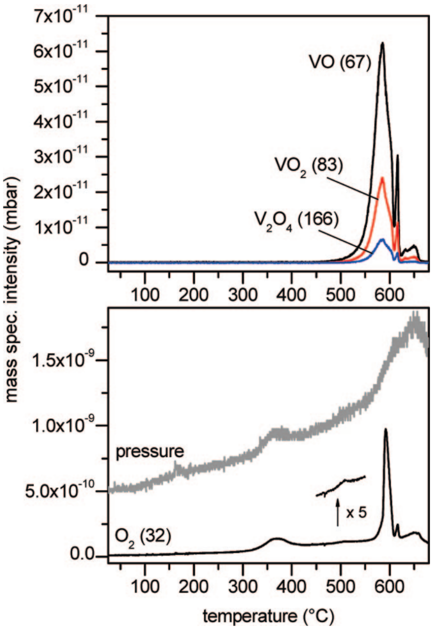

Figure 11. TPD of a $V_2O_5(001)$ film formed by three depositions/oxidation cycles of 2.6 MLE V. The evolution of the main chamber pressure during the TPD run is displayed in the lower graph.

10 mC and annealing at 577 °C for 2 min, no remaining V_2O_5 areas could be found with STM. XPS measurements plotted in Figure 10 indicate the presence of V_2O_3 which leads to the $V2p_{3/2}$ state at 515.15 eV in addition to V_6O_{13} or V_2O_5 giving rise to the peak at 516.9 eV binding energy.[45] Under surface sensitive conditions (electron detection angle at 70° with respect to the surface normal) the latter oxidation state is more prominent than under less surface sensitive conditions (electron detection along the surface normal). This shows that the film consists of a V_6O_{13} surface layer (as observed in STM), whereas deeper layers of the film are reduced to V_2O_3 as a result of diffusion of oxygen to the surface. For the case of a $V_2O_5(001)$ single crystal, similar results were obtained by purely thermal reduction by Blum et al.[58] It this case a single flash at 527 °C was found to lead to a V_6O_{13}-type surface structure (the composition of the bulk was not investigated, but it was assumed it would still consist of V_2O_5) which transformed into a defective $V_2O_3(0001)$-type structure after several cycles of annealing.

b. Thermal Stability. As mentioned previously, the thermal stability of the films under UHV has been investigated with TPD. Figure 11 shows data obtained for a closed $V_2O_5(001)$ film formed by three cycles of deposition and oxidation of 2.6 MLE V, and Figure 12 exhibits data pertaining to a film formed by the oxidation of 5.2 MLE V (a $V_2O_5(001)$ film where some parts of the interface are exposed). Finally, Figure 13 shows the results corresponding to a film with a coverage of less than one monolayer (formed by the oxidation of 0.26 MLE V). It has been shown that such a film forms a well-ordered coincidence structure.[29] The two last sets of TPD curves (Figures 12 and 13) are mainly discussed here to explain some of the features observed in the data obtained for the closed $V_2O_5(001)$ film. For clarity, in all cases the desorption curves have been plotted in two separate graphs (the curves were recorded in the same TPD run). Since the sensitivity of the mass spectrometer for the various gases was not calibrated, the absolute values of the partial pressure should not be given too much significance. However, the signal for each fragment can be compared to some extent from one experiment to the other.

The upper part of Figure 11 reveals that some vanadium oxide fragments are released into the gas phase upon heating a $V_2O_5(001)$ film in the temperature range between 500 and 660 °C. It thus appears that the oxide starts sublimating or decomposing at a temperature of about 500 °C. The V_xO_y desorption spectrum is divided in three regions: a rather broad peak is first observed between 500 and 610 °C, with a maximum at ~585 °C and a clear shoulder around 600 °C. A second very sharp peak appears at a temperature of 616 °C, and a last broad

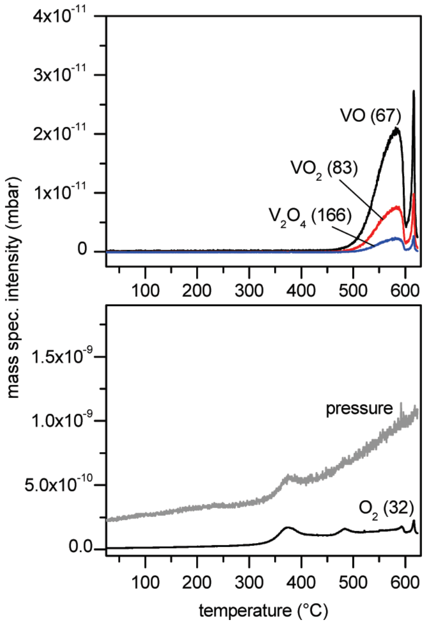

Figure 12. TPD of a $V_2O_5(001)$ film formed by the oxidation of 5.2 MLE V/Au(111).

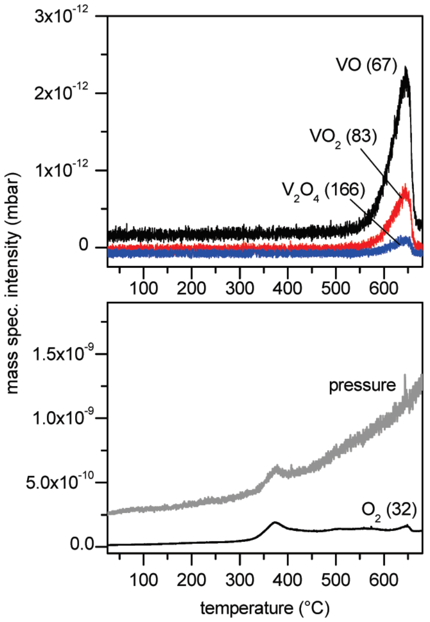

Figure 13. TPD of a film formed by the oxidation of 0.26 MLE V/Au(111).

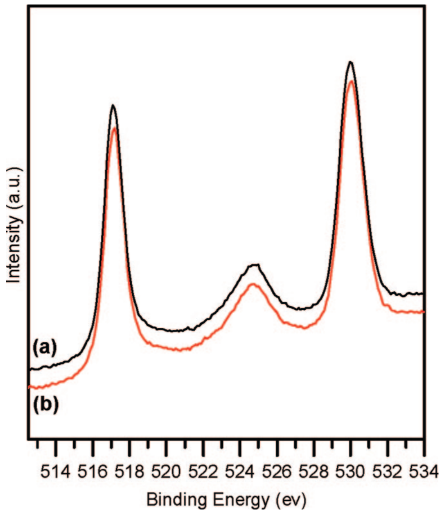

Figure 14. XP spectra (V2p and O1s region) obtained after preparation (a) and following 5 min of annealing in UHV at 450 °C (b) for a film formed by two cycles of deposition and oxidation of 2.6 MLE V/Au(111). The spectra have been shifted with respect to each other in the *y* direction.

desorption region can be observed between 625 and 660 °C. Before discussing these features in more details, the reduction of the film, which should be accompanied by a release of oxygen, will be considered.

The O_2 desorption curve (lower part of Figure 11) contains several peaks. The first broad peak situated between 300 and 420 °C can be attributed to a release of oxygen from the Pt sample holder. In fact, the Pt parts surrounding the sample (see Experimental Methods) are also exposed to 50 mbar O_2 during the oxidation procedure, and they are expected to adsorb considerable amounts of oxygen. It is well-known that O_2 adsorbs dissociatively at room temperature on Pt.[59] The resulting surface O atoms are generally observed to recombine and desorb at temperatures around 300 °C to 600 °C (the exact temperature depends on the surface plane, the coverage, the heating rate, etc).[59,60] The position of the peak observed in our case corresponds quite well to the flash desorption data reported by P. R. Norton for Pt foils exposed to oxygen, where a broad desorption feature starts at about 300 °C.[60] A further argument supporting this assignment comes from the fact that the intensity of the peak is almost the same in the TPD spectra of all the films, including the fractional coverage monolayer (compare Figures 11 and 13). If this O_2 desorption peak would originate from a reduction of the vanadium oxide layer, one would rather expect its intensity to scale somewhat with the thickness of the layer. The Feulner cup used in our experiments shields to some extent the mass spectrometer from the molecules emitted from the surrounding of the sample. However, a significant O_2 release from the sample holder augments the pressure in the UHV chamber and increases the quantity of O_2 molecules that can reach the mass spectrometer detector by passing through the small gap between the Feulner cup entrance and the sample surface (~1 mm).

The O_2 intensity does not fully go down at higher temperatures after the peak and continues increasing on a steady slope. This seems to follow the evolution of the main chamber's pressure. A gradual warm-up of the Pt parts that are further away from the sample and are not directly heated might contribute to the gradual O_2 desorption/pressure increase. In fact, XPS results indicate that no significant reduction of the films takes place at 450 °C. This is evidenced in Figure 14, where spectra acquired after preparation and following heating at 450 °C for 5 min are seen to be identical. The spectra have been slightly shifted along the ordinate axis; otherwise the two curves would be undistinguishable. There is a small O_2 desorption peak at about 500−510 °C which is more clearly visibly after magnification of the intensity scale (see Figure 11). This may be due to a slight oxygen loss of the oxide layer. However, this peak's intensity and desorption temperature varies somewhat from one preparation to the other, which means that it might also originate from the sample holder. The sample holder plate is exposed to oxygen when the sample is oxidized in 50 mbar of oxygen at elevated temperature which means that it probably contains much oxygen.

In contrast to the other O_2 desorption features observed at lower temperatures, a very sharp and intense peak can be seen between 560 and 610 °C in Figure 11. The peak reaches a maximum at ~590 °C and seems to coincide with the intensity decrease of the first V_xO_y desorption feature. As mentioned before, the latter has a high temperature shoulder at about 600 °C. These observations could be interpreted as follows: until ~560 °C, the oxygen loss is negligible while V_2O_5 already starts to sublimate at around 500 °C. However, at ~590 °C a significant loss of oxygen probably accompanied by a structural transition occurs, resulting in a sharp O_2 desorption peak. The resulting reduced phase sublimates/decomposes at a slightly higher temperature than V_2O_5, giving rise to the high temperature shoulder at 600 °C. This phase might consists of V_6O_{13}, which would form via a lattice shear-plane mechanism.[10] Since the sublimation of the V_2O_5(001) layer starts at a lower temperature than the structural transition, one can expect that for smaller thicknesses the sublimation of the V_2O_5(001) layer will be complete before the transition can take place. This seems to be the case for the film produced from 5.2 MLE V. Indeed, as seen in Figure 12 the first broad V_xO_y desorption peak has already lost all its intensity at 600 °C and does not have a clear high temperature shoulder. Concomitantly, the 590 °C O_2 desorption peak is very weak.

The rest of the desorption peaks seen in Figure 11 (610 °C to 660 °C) can possibly be assigned to the decomposition/desorption of the interface film, which is an oxide double-layer.[29] This is supported to some extent by the monolayer film[29] TDS shown in Figure 13 (film formed by the oxidation of 0.26 MLE V), which shows a single wide V_xO_y desorption peak at ~645 °C. This roughly corresponds to the position of the last peak observed in the V_xO_y desorption curves shown in Figure 11. Reduced species formed during the oxygen release at 590 °C can also contribute to some of the desorption intensity observed between 610 and 660 °C.

For all films, XPS revealed that after heating to 680 °C no vanadium (or barely detectable quantities) remains on the Au(111) surface. This observation leads to the conclusion that no significant amount of V_2O_3 is formed during the desorption, since V_2O_3 is stable up to about 750 °C in UHV[27] and would remain on the surface after TPD.

Concerning the removal of oxygen from the thick V_2O_5 films, our results correspond quite well to the TPD data reported by Dziembaj and by Lewis et al.[61–63] Dziembaj's experiments were carried on V_2O_5 powders that were previously degassed and reoxidized *in situ*, while Lewis et al. investigated micron-sized V_2O_5 crystallites that were grown on a gold foil by V_2O_5 evaporation and subsequently fully oxidized in air. In both cases, the release of O_2 was observed to start *slowly* around 450 °C to 500 °C before an intense peak begins to appear at about 550 °C. The observation that only slight oxygen loss takes place below 550 °C to 560 °C also corresponds to the findings of Colpaert and co-workers.[12] In their experiments on V_2O_5 single crystals cleaved in situ, they observed that after heating at 550 °C for 24 h the samples had lost some oxygen, but no structural transition to a lower oxidation state could be detected with either LEED or X-ray diffraction.

A number of studies have been reported on the reduction of V_2O_5 in UHV, and, although the results of the investigations mentioned above agree very well with our findings, some other studies came to various different conclusions. Actually, several authors reported that the reduction of V_2O_5 occurs at much lower temperatures. For instance, Heber and Grünert observed the formation of substantial amounts of V^{4+} species at the surface of polycrystalline V_2O_5 with XPS after annealing at temperatures as low as 200 °C.[57] More recently, Wu et al. also observed a partial surface reduction of evaporated V_2O_5 thin films to V^{4+} at 200 °C.[64] Their photoelectron spectra even revealed the formation of V^{3+} at 400 °C. In both communications, no information concerning the possible formation of crystalline structures of lower oxidation states were reported. In another study, Devriendt and co-workers probed the surface of V_2O_5(001) single crystals annealed at 500 °C with LEED, XPS, and X-ray photoelectron diffraction (XPD).[65] They concluded that V_6O_{13}(001) forms at the surface under those conditions. Only V^{5+} and V^{4+} species were detected with XPS, excluding the presence of V^{3+} at the surface. The thermal reduction of V_2O_5 in UHV has also been investigated with transmission electron microscopy (TEM) by several groups. Su and Schlögl investigated tiny V_2O_5 flakes with TEM and electron energy-loss spectroscopy (EELS).[66] Their samples were already slightly reduced after heating to 200 °C. The EELS spectra and the diffraction patterns indicated a phase transformation into V_2O_3 *via* VO_2: VO_2 was observed at 400 °C, a mixture of VO_2 and V_2O_3 was identified at 500 °C, and only V_2O_3 remained at 600 °C. Ramana et al. did not observe the formation of reduced phases below temperatures of 450 °C during their TEM investigation of thin films grown by evaporation of V_2O_5.[67] However, at 500 °C they identified a phase containing mainly V_2O_5 and smaller amounts of V_2O_3 (V^{3+}) and V_4O_9 (a superstructure with O vacancies in the V_2O_5 lattice [10]). After heating at 600 °C, only V_2O_3 nanocrystals were seen to remain. However, the authors acknowledged that in their case the thermally induced reduction process might have been aided by electron-beam-induced reactions.

From the examples mentioned above, it is obvious that the results on the reduction of V_2O_5 (including both the reduction onset temperature and the observation of structural transitions) vary significantly from one study to the other. This might originate from several complications. First, the presence of surface contamination has been shown to have a critical influence on the reduction process.[12,63] Colpaert et al. detected a significant quantity of carbon contamination at the surface of single crystals that were cleaved in air (not cleaved in the UHV system).[12] Reduction and a structural transition to V_6O_{13} was observed at the surface of these samples after annealing at 550 °C, whereas the carbon-free surface of UHV-cleaved samples retained the V_2O_5 structure after the same thermal treatment (only a "homogeneous" oxygen loss was observed). The difference was attributed to a faster reduction rate at surfaces contaminated with carbon (likely through the formation and desorption of CO and CO_2). If this rate is high enough with respect to the bulk diffusion of O toward the surface, a critical concentration of vacancies can be reached, allowing the nucleation and the growth of V_6O_{13} at the surface through a shear-plane mechanism. Lewis and co-workers also evidenced the fact that the reduction of V_2O_5 is facilitated by the presence of hydrogen atoms or carbon-containing species.[63] Oxygen loss through desorption of water was observed at about 150 °C for surfaces dosed with activated hydrogen. After ethanol adsorption (which was only possible at relatively high exposures), CO and CO_2 were released upon heating around 400 °C. Thus, the surface of contaminated samples will obviously get reduced at lower temperature. In some case, this effect might be even more pronounced since it is foreseeable that V_2O_5 powders and crystals might get bulk-contaminated depending on how they were produced, handled, or stored. Indeed, V_2O_5 has a crystal structure containing rather large cavities, and it is a material that displays good intercalation properties,[4] thereby possibly allowing the inclusion/diffusion of various impurities in its lattice.

Another factor that might partly explain the variance between some of the reduction studies is the marked susceptibility of V_2O_5 to beam damage. As mentioned before, both X-ray[14] and electron beams[12] have been shown to rapidly reduce vanadium pentoxide. In the case of TEM investigations, it thus seems that the contribution of electron beam-induced processes to the observed reduction behavior cannot be fully neglected. Similarly, studies where the samples were exposed to high X-ray doses should be considered with care. In fact, Chenakin et al. showed that significant V^{4+} intensity appears in the V2p XPS signal of V_2O_5 after prolonged Mg Kα exposure.[14]

Even though the reduction experiments mentioned above were carried out with considerably different annealing times, it seems that kinetic factors alone can not explain the divergence of the results. A clear example supporting this affirmation is the fact that Colpaert et al. did not observe significant reduction after annealing 24 h at 550 °C, while Wu et al. reported the formation of V^{3+} following only 1 h of heating at 400 °C.

The observation that V_2O_5 starts to sublimate at about 500 °C in UHV is an interesting result in itself (V_2O_5 has been reported to melt at about 670 °C in ambient conditions[68,69]). To the best of our knowledge, the sublimation of vanadium pentoxide in vacuum has not been investigated in detail yet. Several V_xO_y-type molecules vaporizing from V_2O_5 heated in a Knudsen cell were detected by mass spectrometry by Berkowitz et al.[70] However, the authors did not report at which temperature the material was heated in the Knudsen cell. Farber and co-workers also performed an effusive-mass spectrometric study of the gaseous vanadium compounds evolving from V_2O_5, but their investigated temperature range was limited to 730 °C to 930 °C.[71] Surprisingly, the sublimation of V_2O_5 was not taken into account in any of the studies on the thermal stability mentioned previously. Our results show that V_2O_5 can sublimate before substantial reduction takes place (provided of course that low temperature reduction due to contamination is avoided). This means that in principle, near-stoichiometric films could be grown by the evaporation of V_2O_5. Of course, the evaporation temperature must be kept below the limit where significant reduction occurs (∼560 °C), a condition that most probably severely restrains the achievable evaporation rate. In previous works, much higher evaporation temperatures were sometimes used (for example, 670 °C[64] and 840 °C[16]). In these cases, it is not very surprising that the resulting films were not fully oxidized and contained some V^{4+} species.

Conclusions

Well-ordered V_2O_5(001) thin films containing a low density of point defects can be grown on Au(111) by evaporation of vanadium and subsequent oxidation in 50 mbar O_2. Although the films display some azimuthal disorder, their surface shows rather large (∼20 nm) single crystalline domains and a low density of steps (i.e., the films are “flat”). The growth of such well-ordered V_2O_5(001) thin films with a rather simple technique is interesting and of considerable advantage for the undertaking of model reactivity studies.

The V_2O_5(001) films sublimate at temperatures above 500 °C, whereas significant reduction does not take place until 560 °C and no oxygen loss was detected below 450 °C. Surface contamination appears to drastically influence the thermal reduction of V_2O_5. Considering that V_2O_5 is used as a catalyst because of its ability to transfer oxygen to adsorbed molecules, this is not very surprising.

The susceptibility of V_2O_5 toward X-ray or electron irradiation has also been evidenced in the course of our investigations. The creation of surface vanadyl oxygen vacancies after exposure to X-rays has been probed with STM. The results confirm theoretical predictions[30] that the reduction occurs in a concerted way, the vacancies preferentially appearing in groups (forming rows along [010] and/or pairs along [100]).

Acknowledgment. This work was funded by the Deutsche Forschungsgemeinschaft (DFG) through their Sonderforschungsbereich 546 “Transition Metal Oxide Aggregates”. The Fonds der Chemischen Industrie is gratefully acknowledged for financial support.

References and Notes

(1) Fujita, Y.; Miyazaki, K.; Tatsuyama, C. *Jpn. J. Appl. Phys* **1985**, *24*, 1082.

(2) Nagase, K.; Shimizu, Y.; Miura, N.; Yamazoe, N. *Appl. Phys. Lett.* **1992**, *61*, 243.

(3) Lee, S.-H.; Liu, P.; Tracy, C. E.; Benson, D. K. *Electrochim. Solid-State Lett.* **1999**, *2*, 425.

(4) Lindström, R.; Maurice, V.; Groult, H.; Perrigaud, L.; Zanna, S.; Cohen, C.; Marcus, P. *Electrochim. Acta* **2006**, *51*, 5001.

(5) Hermann, K.; Witko, M. Theory of physical and chemical behavior of transition metal oxides: vanadium and molybdenum oxides In *The chemical physics of solid surfaces*; Woodruff, D. P., Ed.; Elsevier Science: Amsterdam, 2001; *Vol. 9*, Chapter 4 (Oxide Surfaces).

(6) Wachs, I. E.; Weckhuysen, B. M. *Appl. Catal., A* **1997**, *157*, 67.

(7) Weckhuysen, B. M.; Keller, D. E. *Catal. Today* **2003**, *78*, 25.

(8) Grzybowska-Swierkosz, B. *Appl. Catal., A* **1997**, *157*, 263.

(9) Wachs, I. E. *Catal. Today* **1996**, *27*, 437.

(10) Haber, J.; Witko, M.; Tokarz, R. *Appl. Catal., A* **1997**, *157*, 3.

(11) Jachmann, F.; Hucho, C. *Solid State Commun.* **2005**, *135*, 440.

(12) Colpaert, M. N.; Clauws, P.; Fiermans, L.; Vennik, J. *Surf. Sci.* **1973**, *36*, 513.

(13) Zhang, Z.; Henrich, V. E. *Surf. Sci.* **1994**, *321*, 133.

(14) Chenakin, S. P.; Silvy, R. P.; Kruse, N. *J. Phys. Chem. B* **2005**, *109*, 14611.

(15) Julien, C.; Guesdon, J. P.; Gorenstein, A.; Khelfa, A.; Ivanov, I. *Appl. Surf. Sci.* **1995**, *90*, 389.

(16) Murawski, L.; Gledel, C.; Sanchez, C.; Livage, J.; Audières, J. P. *J. Non-Cryst. Solids* **1987**, *89*, 98.

(17) Ramana, C. V.; Smith, R. J.; Hussain, O. M.; Julien, C. M. *J. Vac. Sci. Technol. A* **2004**, *22*, 2453.

(18) Silversmit, G.; Poelman, H.; Gryse, R. D. *Surf. Interface Anal.* **2004**, *36*, 1163.

(19) Wang, X. J.; Li, H. D.; Fei, Y. J.; Wang, X.; Xiong, Y. Y.; Xiong, Y. X.; Nie, Y. X.; Feng, K. A. *Appl. Surf. Sci.* **2001**, *177*, 8.

(20) Groult, H.; Balnois, E.; Mantoux, A.; Van, K. L.; Lincot, D. *Appl. Surf. Sci.* **2006**, *252*, 5917.

(21) Bouzidi, A.; Benramdane, N.; Nakrela, A.; Mathieu, C.; Khelifa, B.; Desfeux, R.; Costa, A. D. *Mater. Sci. Eng., B* **2002**, *95*, 141.

(22) Madix, R. J.; Biener, J.; Bäumer, M.; Dinger, A. *Faraday Discuss.* **1999**, *114*, 67.

(23) Magg, N.; Giorgi, J. B.; Schroeder, T.; Bäumer, M.; Freund, H.-J. *J. Phys. Chem. B* **2002**, *106*, 8756.

(24) Guo, Q.; Lee, S.; Goodman, D. W. *Surf. Sci.* **1999**, *437*, 38.

(25) Sambi, M.; Negra, M. D.; Granozzi, G. *Thin Solid Films* **2001**, *400*, 26.

(26) Dupuis, A.-C.; Haija, M. A.; Richter, B.; Kuhlenbeck, H.; Freund, H.-J. *Surf. Sci.* **2003**, *539*, 99.

(27) Schoiswohl, J.; Sock, M.; Surnev, S.; Ramsey, M. G.; Netzer, F. P.; Kresse, G.; Andersen, J. N. *Surf. Sci.* **2004**, *555*, 101.

(28) Wong, G. S.; Conception, M. R.; Vohs, J. M. *Surf. Sci.* **2003**, *526*, 211.

(29) Guimond, S.; Göbke, D.; Romanyshyn, Y.; Sturm, M.; Naschitzki, M.; Kuhlenbeck, H.; Freund, H.-J. *J. Phys. Chem. C*, in press.

(30) Ganduglia-Pirovano, M. V.; Sauer, J. *Phys. Rev. B* **2004**, *70*, 045422.

(31) Barth, J. V.; Brune, H.; Ertl, G.; Behm, R. J. *Phys. Rev. B* **1990**, *42*, 9307.

(32) Moulder, J. F.; Stickle, W. F.; Sobol, P. E.; Bomben, K. D. *Handbook of X-ray Photoelectron Spectroscopy*; Physical Electronics Division, Perkin-Elmer Corporation: Eden Prairie, MN, 1992.

(33) Fairley, N. CasaXPS version 2.3.10; Casa Software Ltd., 1999−2005.

(34) Feulner, P.; Menzel, D. *J. Vac. Sci. Technol.* **1980**, *17*, 662.

(35) Byström, A.; Wilhelmi, K.-A.; Brotzen, O. *Acta Chem. Scand.* **1950**, *4*, 1119.

(36) Enjalbert, R.; Galy, J. *Acta Crystallogr., Sect. C: Cryst. Struct. Commun.* **1986**, *42*, 1467.

(37) Oshio, T.; Sakai, Y.; Ehara, S. *J. Vac. Sci. Technol. B* **1994**, *12*, 2055.

(38) Goschke, R. A.; Vey, K.; Maier, M.; Walter, U.; Goering, E.; Klemm, M.; Horn, S. *Surf. Sci.* **1996**, *348*, 305.

(39) Smith, R. L.; Lu, W.; Rohrer, G. S. *Surf. Sci.* **1995**, *322*, 293.

(40) Smith, R. L.; Rohrer, G. S.; Lee, K. S.; Seo, D.-K.; Whangbo, M.-H. *Surf. Sci.* **1996**, *367*, 87.

(41) Zimmermann, R.; Claessen, R.; Reinert, F.; Steiner, P.; Hüfner, S. *J. Phys.: Condens. Matter* **1998**, *10*, 5697.

(42) Eyert, V.; Höck, K.-H. *Phys. Rev. B* **1998**, *57*, 12727.

(43) Guimond, S.; Haija, M. A.; Kaya, S.; Lu, J.; Weissenrieder, J.; Shaikhutdinov, S.; Kuhlenbeck, H.; Freund, H.-J.; Döbler, J.; Sauer, J. *Top. Catal.* **2006**, *38*, 117.

(44) Sawatzky, G. A.; Post, D. *Phys. Rev. B* **1979**, *20*, 1546.

(45) Mendialdúa, J.; Casanova, R.; Barbaux, Y. *J. Electron Spectrosc. Relat. Phenom.* **1995**, *71*, 249.

(46) Demeter, M.; Neumann, M.; Reichelt, W. *Surf. Sci.* **2000**, *41*, 454–456.

(47) Silversmit, G.; Depla, D.; Poelman, H.; Marin, G. B.; Gryse, R. D. *J. Electron Spectrosc. Relat. Phenom.* **2004**, *135*, 167.

(48) Kolczewski, C.; Hermann, K. *Surf. Sci.* **2004**, *552*, 98.

(49) Mathieu, C.; Péralta, S.; Costa, A. D.; Barbaux, Y. *Surf. Sci.* **1998**, *395*, L201.

(50) Koma, A. *Thin Solid Films* **1992**, *216*, 72.

(51) Helveg, S.; Lauritsen, J. V.; Lægsgaard, E.; Stensgaard, I.; Nørskov, J. K.; Clausen, B. S.; Topsøe, H.; Besenbacher, F. *Phys. Rev. Lett.* **2000**, *84*, 951.

(52) Hermann, K.; Witko, M.; Druzinic, R.; Chakrabarti, A.; Tepper, B.; Elsner, M.; Gorschlüter, A.; Kuhlenbeck, H.; Freund, H. J. *J. Electron Spectrosc. Relat. Phenom.* **1998**, *245*, 98–99.

(53) Tepper, B.; Richter, B.; Dupuis, A.-C.; Kuhlenbeck, H.; Hucho, C.; Schilbe, P.; Yarmo, M. A.b.; Freund, H.-J. *Surf. Sci.* **2002**, *496*, 64.

(54) Cazaux, J. *J. Electron Spectrosc. Relat. Phenom.* **1999**, *105*, 155.

(55) Haija, M. A.; Guimond, S.; Uhl, A.; Kuhlenbeck, H.; Freund, H.-J. *Surf. Sci.* **2005**, *600*, 1040.

(56) Hermann, K.; Witko, M.; Druzinic, R.; Tokarz, R. *Appl. Phys. A: Mater. Sci. Process.* **2001**, *72*, 429.

(57) Heber, M.; Grünert, W. *J. Phys. Chem. B* **2000**, *104*, 5288.

(58) Blum, R.-P.; Niehus, H.; Hucho, C.; Fortrie, R.; Ganduglia-Pirovano, M. V.; Sauer, J.; Shaikhutdinov, S.; Freund, H.-J. *Phys. Rev. Lett.* **2007**, *99*, 226103.

(59) Derry, G. N.; Ross, P. N. *Surf. Sci.* **1984**, *140*, 165.

(60) Norton, P. R. *Surf. Sci.* **1975**, *47*, 98.

(61) Dziembaj, R. *Bull. Acad. Polon. Sci.* **1976**, *24*, 965.

(62) Dziembaj, R. *React. Kinet. Catal. Lett.* **1978**, *9*, 389.

(63) Lewis, K. B.; Oyama, S. T.; Somorjai, G. A. *Appl. Surf. Sci.* **1991**, *52*, 241.

(64) Wu, Q.-H.; Thissen, A.; Jaegermann, W.; Liu, M. *Appl. Surf. Sci.* **2004**, *236*, 473.

(65) Devriendt, K.; Poelman, H.; Fiermans, L. *Surf. Sci.* **1999**, *734*, 433–435.

(66) Su, D. S; Schlögl, R. *Catal. Lett.* **2002**, *115*, 3–4.

(67) Ramana, C. V.; Utsunomiya, S.; Ewing, R. C.; Becker, U. *Solid State Commun.* **2006**, *137*, 645.

(68) *Gmelins Hanbuch der Anorganischen Chemie*, 8th ed.; Gmelin-Institut, Ed.; Verlag Chemie GmbH: Weinheim (Germany), 1967; *Vol. 48 B1*.

(69) *CRC Handbook of Chemistry and Physics*, 84th ed.; Lide, D. R., Ed.; CRC Press: New York, 2003−2004.

(70) Berkowitz, J.; Chupka, W. A.; Inghram, M. G. *J. Chem. Phys.* **1957**, *27*, 87.

(71) Farber, M.; Uy, O. M.; Srivastava, R. D. *J. Chem. Phys.* **1972**, *56*, 5312.

JP8011156